

# Gated CRF Loss for Weakly Supervised Semantic Image Segmentation

Anton Obukhov<sup>1</sup>, Stamatis Georgoulis<sup>1</sup>, Dengxin Dai<sup>1</sup>, Luc Van Gool<sup>1,2</sup>

<sup>1</sup> ETH Zürich, <sup>2</sup> KU Leuven

{anton.obukhov,stamatis.georgoulis,dai,vangool}@vision.ee.ethz.ch

## Abstract

State-of-the-art approaches for semantic segmentation rely on deep convolutional neural networks trained on fully annotated datasets, that have been shown to be notoriously expensive to collect, both in terms of time and money. To remedy this situation, weakly supervised methods leverage other forms of supervision that require substantially less annotation effort, but they typically present an inability to predict precise object boundaries due to approximate nature of the supervisory signals in those regions. While great progress has been made in improving the performance, many of these weakly supervised methods are highly tailored to their own specific settings. This raises challenges in reusing algorithms and making steady progress. In this paper, we intentionally avoid such practices when tackling weakly supervised semantic segmentation. In particular, we train standard neural networks with partial cross-entropy loss function for the labeled pixels and our proposed Gated CRF loss for the unlabeled pixels. The Gated CRF loss is designed to deliver several important assets: 1) it enables flexibility in the kernel construction to mask out influence from undesired pixel positions; 2) it offloads learning contextual relations to CNN and concentrates on semantic boundaries; 3) it does not rely on high-dimensional filtering and thus has a simple implementation. Throughout the paper we present the advantages of the loss function, analyze several aspects of weakly supervised training, and show that our ‘purist’ approach achieves state-of-the-art performance for both click-based and scribble-based annotations.



Figure 1: Original image from Pascal VOC validation set, and semantic segmentation predictions, made by models trained with full, scribbles, and clicks supervision respectively. The proposed Gated CRF loss is a step towards bridging the gap between weak and full supervision. Best viewed in color.

## 1 Introduction

Semantic image segmentation is of great importance because of its many applications. To achieve state-of-the-art performance in this task, deep models [23] of fully convolutional networks [40] are typically trained on datasets, such as PASCAL VOC 2012 [16], MS COCO [38], and Cityscapes [13], that contain a large number of fully-annotated images. However, obtaining accurate, pixel-wise semantic labels for every image in such a dataset is a labor-intensive process that costs significant amounts of time and money, as shown in [4].

To remedy this situation, weakly-annotated methods leverage other forms of supervision - in particular partial inputs like scribbles [60, 37, 59, 55, 56], bounding boxes [44, 60, 14, 29], clicks [4], and image-level tags [44, 60, 56, 2] – that require substantially less annotation effort. Unfortunately, this comes at the cost of segmentation performance, and is largely attributed to imprecise object boundaries predictions due to the lack of enough supervisory signals in these regions. To overcome this issue, most approaches combine traditional segmentation techniques, like graph cuts [7, 53], with boxes or seeds to produce ‘fake’ semantic labels (i.e. proposals) outside the partial inputs. They consequently treat these proposals as ground-truth and train CNNs in an iterative manner, e.g. alternating CNN training with proposal generation [44, 37, 29]. In a different vein, Tang et al. [55, 56] proposed to fine-tune conventional segmentation models using regularized losses (e.g. based on relaxations of conditional random fields (CRF) potentials) over the whole image, after pre-training them with standard losses over the partial inputs, which leads to improved performance.

In general, previous weakly-supervised methods rely on alternative sources of supervision, be it generation of segmentation proposals [44, 37, 29, 2], enlargement of the annotated inputs [37], priors from other tasks [4], pre-training on other datasets [55, 56], or employ unconventional training procedures [41], in their effort to minimize the gap between weakly- and fully-supervised segmentation performance. While considerable progress has been made, the introduced modules in many of the previous methods are tailored to their specific settings, which limits the possibility of reusing algorithms and making steady progress in this field. In this work, we aim for a simple, yet effective, learning method to study the fundamental problem of weakly supervised semantic segmentation.

To realize this concept, we propose to train conventional segmentation architectures while jointly minimizing partial cross-entropy on the weak annotations and the proposed Gated CRF loss for the non-annotated parts. Similarly to [55, 56], the Gated CRF loss belongs to the group of *regularized losses*, originally motivated by multi-decade research on designing regularizers [17, 5, 27, 43, 8, 6] based on geometry, physics, etc. that exploit the structural similarity of partially annotated or non-annotated data. In contrast, the proposed Gated CRF loss (1) enables flexibility in the kernel construction, masking out undesired contributions to the loss; (2) offloads learning contextual relations to CNN and concentrates on semantic boundaries; (3) simplifies the combination of CRF and modern neural networks in a single-stage training; (4) does not rely on high-dimensional filtering [1] for the computational part, which allows for a GPU-based implementation, and thus, a seamless integration with modern neural networks. In the following sections we provide more insights in several aspects of the weakly-supervised training and show that our ‘purist’ approach achieves state-of-the-art performance for clicks and scribbles annotations, bringing weakly-supervised semantic segmentation closer to the fully-supervised one (see Fig. 1). Upon publication, we will provide source code for our loss function, for use with major deep learning frameworks.

## 2 Related work

**Graphical models for segmentation.** Before the deep learning era, graphical models, like MRF and CRF, had been the ‘go-to approach’ when it came to interactive image segmentation [7, 53, 36, 20, 35] as well as semantic segmentation [34, 54, 30, 32]. Simply put, these are probabilistic models defined on a graph that leverage unary and pairwise potentials to model local or global dependencies between graph nodes. In segmentation this means that if two nodes, i.e. pixels, have larger graph affinity, then they are encouraged to have the same label. By doing so, object boundaries are better delineated. The concept of regularized losses, which is also adopted in this paper, is inspired by graphical models. Yet, instead of utilizing graphical models in conjunction with CNNs (as post-processing or for joint training), which is computationally expensive, their pairwise potentials are directly expressed as a loss function, simplifying CNN training.

**Fully-supervised segmentation.** The deep learning era in semantic segmentation started when Long et al. [40] introduced the fully convolutional networks by replacing the fully connected layers in existing classification models with convolutional ones. This enables the network to produce dense outputs of any size. Many works followed that tried to: (1) leverage local information in order to improve pixel-wise accuracy, (2) integrate global context information in order to resolve local ambiguities, (3) integrate both of the above. The most representatives ones include the use of encoder-decoder architectures [3, 12], dilated or atrous convolutions [61, 9, 10, 12], pyramid pooling modules [63], multi-scale predictions [15, 62], feature fusion [39, 50], attention models [11, 24], adaptive affinity fields [28], etc. These approaches achieve highly-accurate segmentation results by

leveraging the ability of deep models to learn complex image representations when trained on datasets with a large number of fully-annotated images, such as PASCAL VOC 2012 [16], MS COCO [38], Cityscapes [13], and ADE20K [64]. However, generating accurate, pixel-wise semantic labels for every image in such a dataset is a labor-intensive process that costs both time and money [4].

**Weakly-supervised segmentation.** To bypass the heavy annotation burden weakly-supervised methods have opted for less expensive forms of supervision. The most popular alternatives include partial inputs like scribbles [60, 37, 59, 55, 56], bounding boxes [44, 60, 14, 29], clicks [4], and image-level tags [44, 60, 56, 2]. The majority of weakly-supervised works [14, 37, 29, 44, 31, 47, 59, 52, 2] try to mimic their fully-supervised counterparts by generating ‘fake’ semantic labels (i.e. proposals) which are consequently used as ground truth. In particular, they train CNN models to fit these generated proposals using cross-entropy or modified versions of it, and alternate between the CNN training and proposal generation steps. To generate the object proposals different techniques have been used, such as graph cuts [7, 37], CRF layers [31], cardinality constraints [47], or generally any heuristic segmentation algorithm [36, 53, 51, 29]. As shown in [55, 56], however, the inherent mistakes present in the generated ‘fake’ proposals tend to reinforce themselves in a self-learning scheme, that has no convergence guarantee, leading to over-fitting. Instead of generating unreliable proposals and training networks to fit them, Tang et al. [55] propose to combine the minimization of a partial cross-entropy loss for the labeled pixels with regularized losses, particularly normalized cuts, for the unlabeled pixels. They extended their work in [56] to incorporate standard regularization techniques for image segmentation, e.g. graph cuts or dense CRFs, directly into the loss functions over the partial inputs. In general, the aforementioned methods rely on alternative sources of supervision, be it the generation of segmentation proposals [44, 37, 29, 2], enlargement of the annotated inputs [37], priors from other tasks [4], pre-training on other datasets [55, 56], or employ unconventional training procedures [41], in order to minimize the performance gap between weakly- and fully-supervised semantic segmentation. While great progress is made, many of these methods are highly tailored to their own specific settings, which raises challenges in reusing algorithms and making steady progress. In contrast, we avoid such practices and aim for a simple, yet very effective, method in this paper.

### 3 Method

**Cross-entropy for semantic segmentation.** Training a neural network  $\mathcal{F}$  for the task of semantic segmentation requires pairs of images  $x$  with their annotated counterparts  $y$ , conveying per-pixel class assignments from  $C$  classes. Let us denote with  $N$  the total number of pixels in an image, positions of pixels with subscripts, and the probability of class  $i$  in the prediction  $\hat{y} = \mathcal{F}(x)$  as  $\hat{y}_i$ . The conventional loss for multi-class classification problems is the cross-entropy loss, which takes the form  $\mathcal{L}_{\text{CE}}(\hat{y}_i, y_i) = -\sum_{c=1}^C y_i(c) \log \hat{y}_i(c)$  when  $y$  is given as a probability distribution, or  $\mathcal{L}_{\text{CE}}(\hat{y}_i, y_i) = -\log \hat{y}_i(y_i)$  when  $y$  takes on class labels.

In the fully-supervised setting, nearly all pixels of the training images are annotated, forming a dense map of annotated pixels  $m_i \in \{0, 1\}$  of the same size as  $y$ , with possible unannotated exceptions including ambiguous or irrelevant classes (e.g. the ego-vehicle [13], frame boundaries, etc.). In the weakly-supervised setting, only a few pixels of the training images are annotated, forming a partial map of annotated pixels  $m_i$ , whose sparsity depends on the type of weak annotation (e.g. scribbles, clicks). Since the unannotated pixels present no information to the learning process, they are left out of consideration in the loss function, used to compute gradients with back-propagation, i.e.  $\mathcal{L}_{\text{CE}}(\hat{y}, y) = \sum_{i=1}^N m_i \mathcal{L}_{\text{CE}}(\hat{y}_i, y_i) / \sum_{i=1}^N m_i$ . Note that, in the literature the cross-entropy loss for weakly-supervised semantic segmentation is usually called partial cross-entropy (pCE) due to the partial maps of annotated pixels  $m_i$ . Here, we also adopt this notion.

**Weak annotations: scribbles & clicks.** A typical weakly-supervised setting is driven by the motivation to annotate fewer pixels while obtaining more samples. Drawing polygons, scribbles, or bounding boxes has been shown to yield a good compromise between annotation time and segmentation performance [4, 37, 13]. In contrast to bounding boxes, clicks and scribbles have a few valuable assets: 1) while being sparse, the annotated pixels are more accurate and reliable; 2) the annotation process is more efficient; and 3) object classes and stuff classes (e.g. “sky”, “road”) can be handled the same way. Therefore, in this work, we focus on click and scribble annotations, but the proposed techniques can also be applied for e.g. image-level tags by replacing pCE with an appropriate loss.

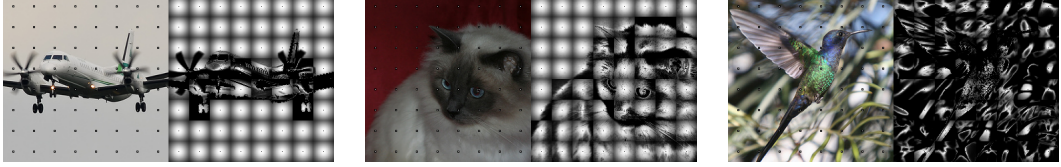


Figure 2: Examples of images from the Pascal VOC dataset, and the corresponding Gaussian kernels (RGBXY with  $\sigma_{\text{RGB}} = 0.1$ ,  $\sigma_{\text{XY}} = 12.0$ ), computed in the square neighborhoods (31x31 pixels) of the marked central pixels (anchors). White filter pixels encode higher energy of assigning a label other than the label of the corresponding anchor. The stride between anchors is 31 pixels in this visualization, however in Gated CRF loss the stride is 1.

**Gated CRF loss for dense labeling tasks.** As already mentioned, we set out to find a method to minimize the performance gap between weakly- and fully-supervised semantic segmentation. We want to achieve this without relying on any of the commonly used priors, e.g. "objectness" [4]; without enlarging the annotated inputs [37]; without pre-training models on a similar task and dataset (i.e. COCO) [55, 56]; without using complex training procedures [55, 56, 42] or optimizing the network weights with unconventional minimization techniques [41]; and without generating 'fake' proposals as ground truth [44, 37, 29, 2] and training for multiple rounds [14], which was shown to lead to overfitting [55]. Since just applying pCE on weak annotations usually does not provide enough supervision signal close to semantic boundaries, it is natural to expect worse predictions where this supervision is unavailable. To alleviate that, we use the annotated inputs as seeds of supervision signal for pCE, and propagate it to the surrounding pixels with other forms of regularization. This approach has proven to work in both classical CRF post-processing [32] as well as a loss function [56]. Yet, we are constraining our setting to a single round of joint training with no pre-/post-processing operations.

Similarly to [26], we first define the energy term of labeling classes  $i$  and  $j$  at positions  $a$  and  $b$ , as:

$$\psi_{a,b}(i, j) = \mu(i, j) K_{ab} \quad \text{s.t.} \quad K_{ab} = \sum_{p=1}^P w^{(p)} k^{(p)}(f_a^{(p)}, f_b^{(p)}), \quad (1)$$

where  $\psi_{a,b}$  denotes the pairwise potentials [32, 26], and  $\mu$  is a generic class compatibility matrix of size  $\mathbb{R}^{C \times C}$ , followed by a mixture of  $P$  kernels  $k^{(p)}(\cdot, \cdot)$  for a pair of positions with weights  $w^{(p)}$ . The feature vector  $f_a^{(p)}$  is specific to the  $p$ -th kernel, and does not depend on the prediction; in practice it often consists of position coordinates or input modalities, such as RGB or depth. Following the established practice in [32], we use Gaussian kernels with kernel-specific bandwidth parameters  $\sigma^{(p)}$  and Pott's class compatibility model:

$$k^{(p)}(f_a^{(p)}, f_b^{(p)}) = \exp \left\{ -\frac{1}{2} \left| \frac{f_a^{(p)} - f_b^{(p)}}{\sigma^{(p)}} \right|^2 \right\} \quad \mu(i, j) = \begin{cases} 0, & \text{if } i = j \\ 1, & \text{otherwise.} \end{cases} \quad (2)$$

Looking into the defined energy term, it is apparent that its value is higher if the labeling of classes at two positions is different given its feature-wise similarity. This similarity is defined by the combination, weights and bandwidths of the kernels, which in the case of a single bilateral (RGBXY) kernel translates into 5D color-proximity similarity – a few examples are shown in Fig. 2.

The formulation of labeling energy in Eq. 1 is amenable to continuous relaxation [26], which is a desired property of a loss function taking class probabilities. We can now write the energy of prediction  $\hat{y}$  at positions  $a$  and  $b$ , and subsequently the total energy of the prediction  $\hat{y}$  in a "dense" setting, where every pixel of the image is related to every other:

$$\psi_{a,b}(\hat{y}) = \sum_{i,j \in [1,C]} \psi_{a,b}(i, j) \hat{y}_a(i) \hat{y}_b(j) \quad \Psi(\hat{y}) = \sum_{a=1}^N \sum_{\substack{b=1 \\ b \neq a}}^N \psi_{a,b}(\hat{y}) \quad (3)$$

This energy formulation of the prediction  $\hat{y}$  is the central part of CRF and has been adopted in previous works [55, 56, 41]. While improvements have been made, there are several important aspects which are still missing when instantiating this energy formulation for weakly supervised semantic segmentation. These observations motivate our Gated CRF loss, and are summarized below:

(1) The  $b \neq a$  condition specifies that the total energy term excludes the energy of self-labeling. However, there are other pixel positions than just the self-position  $a$  that one may want to exclude from the total energy. Examples could be pixels marked as invalid, be it over-/under-exposed regions in RGB images or missing data in other modalities such as depth maps. The 'to-be-excluded' regions can also be generated by some commonly used computational operations, such as the out-of-bound regions of RGB images produced through data augmentation (image cropping and rotation) of deep learning frameworks. In order to exclude these pixels from influencing other pixels, we define a source map  $m_a^{src}$  of the same size as the image  $x$ , where  $m_a^{src} \in \{0, 1\}$  with 1 indicating pixels that can be used to provide a pairwise energy to any other positions in the image and 0 otherwise.

(2) Summation over all positions  $a \in [1, N]$  makes the assumption that the total energy is found as such accumulation. This is also an over-simplification for some cases, including weakly-supervised segmentation. For this task, it might be desirable to exclude the annotated positions from receiving influences from other pixels, as the pCE loss delivers a direct and much stronger supervision in these positions. Simply put, applying the CRF energy term to 'correct' the labels of the annotated pixels brings in no additional benefits if they are classified correctly by pCE. In order to exclude these pixels from receiving energy, we define a destination map  $m_a^{dst}$  of the same size as the image  $x$ , where  $m_a^{dst} \in \{0, 1\}$  with 1 indicating pixels that can be used to receive and accumulate a pairwise energy from any other positions in the image and 0 otherwise.

(3) For any fixed position  $a$ , the pairwise energy of jointly labeling  $a$  and  $b$  will diminish with the distance from  $a$ , assuming that all kernels are Gaussian and the feature vectors  $k^{(p)}$  contain position coordinates. A CRF loss with a long range of summation poses great computational challenges for the joint training of deep neural networks with the combination of pCE and CRF losses. This is especially the case when the supervision signals are very sparse and weak. We argue that the "dense" property of the CRF setting in [32] used to be vital for capturing long-range relations between pixels, when employed together with the fairly simple unary term models [54]. Modern predictive models based on CNNs evolved dedicated mechanisms, which capture the global context efficiently [9]. Hence, having dense pairwise terms may not bring extra benefit. What's more, this calls for using high-dimensional filtering techniques [1] to alleviate prohibitive computational complexity, which also perplexes manipulations with the kernel terms. We argue that in the context of weakly-supervised semantic segmentation, it is therefore beneficial to limit the range of summation of  $b$  to a local neighborhood  $\Omega(a)$  characterized by a function of the acceptable loss of signal  $\epsilon$  and kernel bandwidth  $\sigma^{(p)}$ .

To address observations (1) and (2), we reformulate Eq. 1 to support gated information propagation:

$$\psi_{a,b}(i, j) = \mu(i, j) G_{ab} K_{ab}, \quad (4)$$

where  $G_{ab} = m_a^{dst} m_b^{src}$  is our gate function, which allows us to selectively sum up the energies – energy from position  $b$  to position  $a$  is considered only if  $b$  is a valid 'source' position and  $a$  is a valid 'destination' position. Following up on observation (3), we define the two-dimensional local neighborhood window with radius  $r$  of a position  $a$  (having coordinates  $a_x, a_y$ ) as  $\Omega_r(a) = [a_x - r, a_x + r] \times [a_y - r, a_y + r]$ . The total energy then becomes:

$$\Psi(\hat{y}) = \sum_{a=1}^N \sum_{b \in \Omega_r(a) \setminus \{a\}} \psi_{a,b}(\hat{y}) \quad (5)$$

The latter representation can be computed efficiently using standard tensor operations (see supplementary material). Because the loss function is embedded directly into the network, local influences are propagated to the whole range of the image during training.

Our proposed Gated CRF loss function is just the total energy of the predicted class probabilities:  $\mathcal{L}_{GCRF}(\hat{y}) = \Psi(\hat{y}) / \sum_{i=1}^N m_i^{dst}$ . In all experiments the contribution of the Gated CRF loss to the final loss value is defined by a hyperparameter  $\lambda$ :  $\mathcal{L}(\hat{y}) = \mathcal{L}_{CE}(\hat{y}, y) + \lambda \mathcal{L}_{GCRF}(\hat{y})$ .

## 4 Experiments

### 4.1 Our setup

**CNN backbone.** Gated CRF loss does not rely on any specific architecture, and can be used directly on the prediction layer of any CNN backbone. We chose the DeepLab-v3plus [9] network for its flexibility in the choice of encoder, rich context sharing ASPP module, and a simple decoder.

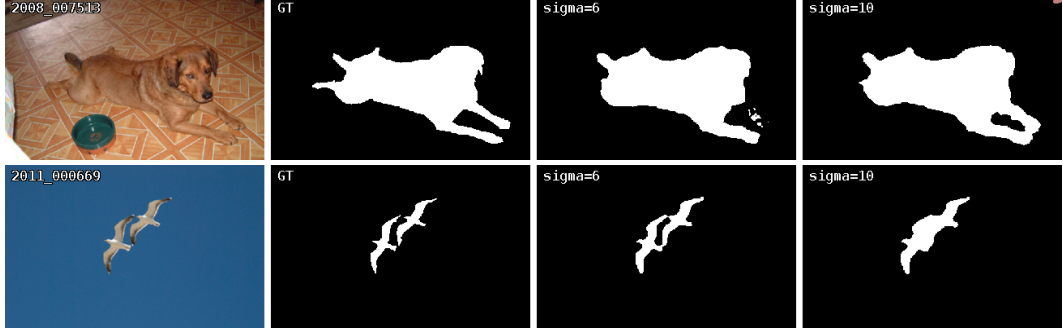


Figure 3: Effect of increasing  $\sigma_{XY}$  during training: thin structures are learned better (top row) at the cost of boundaries precision (bottom row). Left to right: input images, dense annotations, predictions of models trained with  $\sigma_{XY} = 6$  and  $\sigma_{XY} = 10$ . Only the class of interest is recolored in white.

**Training details.** We follow the same training procedure as in DeepLab-v3plus [12]. In particular, we employ a lightweight form of that network: For encoding, ResNet-34 was chosen as a trade-off between performance under full supervision and its relatively small number of weights, leaving more than half of total GPU memory (12Gb) for the needs of Gated CRF loss, without sacrificing batch or crop sizes. The output stride of the encoder is set to 16 and ASPP [9] atrous rates are (6, 12, 18). We train the model using SGD with base learning rate  $7e^{-3}$ , polynomial schedule [39]  $LR = LR_{base}(1 - progress)^{0.9}$ , momentum of 0.9, and weight decay of  $1e^{-4}$ , for 90K steps. We initialize the ResNet layers using the pre-trained weights from ILSVRC [33], as commonly done in weakly-supervised segmentation approaches [18, 44, 40, 48, 49, 9]. Although ImageNet pretraining of the encoder is found to be helpful for faster convergence, it is not entirely necessary, provided the dataset is large enough and longer training cycles are acceptable [22]. To bring the distribution of the input closer to what the encoder was pre-trained with, all RGB inputs to the network are standardized using the training split statistics. For all remaining layers we use Xavier [19] initialization. We keep all BatchNorm [25] layers trainable. Data augmentations are limited to those of [9] and include cropping with random scale in [0.5, 2.0], and random horizontal flipping.

**Datasets and metrics.** We use two datasets and their derivatives to demonstrate the capabilities and limitations of the proposed loss function. The majority of experiments are conducted on Pascal VOC 2012 [16, 21], which is composed of 10582 photos in the training and 1449 in the validation splits, and their corresponding dense semantic annotations with 21 classes. For our experiments in this dataset, we utilize the scribble annotations provided by ScribbleSup paper [37] as well as the click annotations from What’s the point paper [4] (for more details we refer the reader to the supplementary material). A smaller subset of experiments is done on CityScapes [13], that contains 2975 urban driving scene photos in the training and 500 photos in the validation splits, and their corresponding dense semantic annotations with 19 classes. Since there are no publicly available weak annotations for this dataset we simulate clicks annotations from the dense annotations (please visit the supplementary material for details). For both datasets, we report mean intersection over union (mIoU) [40] over validation splits as the performance metric.

**Mini-batch assembly.** We adjust the strategy of mini-batches assembly according to the dataset at hand. It has been shown [10], albeit in the fully-supervised case, that larger crop sizes help the network equipped with a context aggregation module to learn long range relations better. For CityScapes, which consists of images with resolution  $1024 \times 2048$ , in order to efficiently utilize the crops and given the random scaling augmentation discussed above, we chose a crop size of  $768 \times 768$ . Such choice permits a mini-batch of 8 samples to fit in one conventional GPU. The structure of Pascal VOC is different: unlike the dense urban setting with many relevant classes neighboring at different scales, a typical Pascal VOC image is smaller than  $512 \times 512$  pixels (a baseline crop size from [9]), and contains just a few framed foreground objects over the background. Considering this, we chose to use smaller crop size of  $256 \times 256$ , but larger batch of size 48.

**Gated CRF loss configuration.** We apply the proposed loss function over the logits output of the model (which is 4x smaller than the original resolution), followed by the softmax operation to produce

class probabilities. The local neighborhood size is set to 11 pixels. We utilize a single Gaussian kernel with RGBXY feature vectors with  $\sigma_{\text{RGB}} = 0.1$ ,  $\sigma_{\text{XY}} = 6$ , kernel weight  $w = 1$ .

## 4.2 Ablation studies

In this section, we show that source masking is crucial to achieving high quality segmentation, and that increasing the local neighborhood size together with  $\sigma_{\text{XY}}$  does not give quality improvement. All reported mIoUs are on the validation sets. Larger values are better, best values are in bold. Supervision icons:  $\blacktriangleleft$  – clicks (or disks with radius),  $\wp$  – scribbles,  $\blacksquare$  – bounding boxes,  $\blacksquare$  – full supervision.

**Source and destination masking.** Table 1 shows mIoU scores for 4 combinations of losses (pCE, pCE+GCRF, pCE+GCRF<sub>s</sub>, pCE+GCRF<sub>s,d</sub>) at each of 3 levels of supervision (clicks, scribbles, full), on 2 datasets (Pascal VOC, Cityscapes). Note that, destination masking with full supervision is omitted due to null set of pixels for the Gated CRF loss. We observe that source masking consistently improves mIoU under all methods of weak supervision. Further adding destination masking gives approximately 1% improvement in Cityscapes, but up to 0.20% deterioration in Pascal VOC. This can be explained by the nature of the weak annotations in both datasets. Cityscapes usually contains many instances of objects scattered around the image. This provides enough weak annotations for the pCE alone to learn strong class descriptions. As a result, activating destination masking in this case makes sense as it would suppress the effect of Gated CRF loss over the more reliable pCE. However, in Pascal VOC typically only a few instances of objects exist in an image. As such, weak annotations are far less and more sparse compared to Cityscapes, making supervision from pCE less reliable. In this case, deactivating destination masking seems a better choice as it would prioritize Gated CRF loss over the less reliable pCE. We conclude that source masking should be the de facto case, whereas destination masking should be decided in a dataset-to-dataset case.

**Enlargement of annotated inputs.** Table 2 conveys that even a seemingly insignificant increase in the size of point supervision from  $[1 \times 1]$ px to  $[3 \times 3]$ px, as done by many existing approaches, produces models which differ by 3% mIoU for the baseline case, i.e. only pCE. However, our Gated CRF loss used together with pCE in the same setting manages to bridge this gap, even when using only  $[1 \times 1]$ px supervision.

Furthermore, arbitrarily enlarging the annotated input is not always beneficial, as it hints to prior knowledge about the minimum size of objects which largely varies between datasets. For example, we observe that using only pCE on CityScapes does not improve from  $[1 \times 1]$ px to  $[3 \times 3]$ px, possibly because enlarging the annotations of very small objects in the background overpopulates other classes.

**Local neighborhood size.** Table 3 demonstrates the effect of varying  $\sigma_{\text{XY}}$  together with proportionally adjusting the local neighborhood size. It can be seen that validation performance does not

Table 1: Results of training with pCE, and 3 combinations of masking with the proposed Gated CRF loss (subscripts of GCRF).

		pCE	GCRF	GCRF <sub>s</sub>	GCRF <sub>s,d</sub>
VOC	$\blacktriangleleft$	48.97	59.99	<b>67.39</b>	67.29
	$\wp$	67.38	72.73	<b>75.50</b>	75.29
	$\blacksquare$	76.68	76.64	<b>77.16</b>	—
CS	$\blacktriangleleft$	38.61	51.33	56.46	<b>57.43</b>
	$\blacksquare$	76.06	<b>76.88</b>	75.38	—

Table 2: Effect of enlarging the annotated click.  $[1 \times 1]$ px clicks provide the bare minimum of supervision, whereas  $[3 \times 3]$ px enlarge supervision by 8 pixels. Gated CRF loss bridges this gap.

		pCE	GCRF
VOC	$\blacktriangleleft$ - $[3 \times 3]$ px	51.86	66.87
	$\blacktriangleleft$ - $[1 \times 1]$ px	48.97	67.39
CS	$\blacktriangleleft$ - $[3 \times 3]$ px	38.31	56.53
	$\blacktriangleleft$ - $[1 \times 1]$ px	38.61	56.46

Table 3: Effect of varying bandwidth of the kernel’s spatial component. The values suggest that longer range relations may not play important role in CNN training setting.

		$\sigma_{\text{XY}} = 3$	$\sigma_{\text{XY}} = 6$	$\sigma_{\text{XY}} = 10$
VOC	$\blacktriangleleft$	66.21	<b>67.39</b>	66.44
	$\wp$	75.21	<b>75.50</b>	74.08

Table 4: Ablation of loss weight  $\lambda$ .

	0.05	0.1	0.15	0.2	0.3
VOC	$\blacktriangleleft$	65.98	<b>67.39</b>	67.29	66.89
	$\wp$	75.05	<b>75.50</b>	74.67	73.60
	$\blacksquare$	76.77	77.16	<b>77.18</b>	76.92

Table 5: Performance comparison on Pascal VOC dataset ( $\bowtie$  – clicks (or disks with radius),  $\square$  – bounding boxes,  $\bowtie$  – scribbles). Best values are in bold.

Paper	Specifics	Weak (mIoU)	Full (mIoU)	W/F (%)
$\bowtie$ What’s the point [4]	vgg16, size=1px, objectness prior	43.40	58.30	74.44
$\bowtie$ ScribbleSup [37]	deeplab-v2-vgg16, size=3px, proposals	51.60	68.50	75.32
$\bowtie$ Regularized loss [56]	deeplab-v2-resnet101, size=3px, COCO	57.00	68.70	82.96
$\bowtie$ <b>Gated CRF loss</b>	deeplab-v3plus-resnet34, size=1px	<b>67.39</b>	76.68	<b>87.88</b>
$\bowtie$ ScribbleSup [37]	deeplab-v2-vgg16, stroke=3px, proposals	63.10	68.50	92.11
$\bowtie$ Regularized loss [56]	deeplab-v2-resnet101, stroke=3px, COCO	72.90	75.60	96.42
$\bowtie$ <b>Gated CRF loss</b>	deeplab-v3plus-resnet34, stroke=3px	<b>75.50</b>	76.68	<b>98.46</b>
$\square$ Simple does it [29]	deeplab-v1-vgg16, proposals, heuristics, multiple training rounds	65.70	72.30	90.87
$\square$ Simple does it [29]	deeplab-v2-resnet101, proposals, heuristics, multiple training rounds	69.40	74.50	93.15

consistently increase as  $\sigma_{XY}$  become larger, which hints that our locally applied loss has a global effect even for small  $\sigma_{XY}$ , as discussed in Sec. 3. Nevertheless, some long thin structures are still learned better for larger  $\sigma_{XY}$ , at the cost of a few other classes score (see Fig. 3).

**Gated CRF loss weight.** Table 4 shows the effect of using different Gated CRF loss weight  $\lambda$  with 3 levels of supervision on Pascal VOC. The chosen value of  $\lambda = 0.1$  gives the best overall results. However, we also observe that, at least for the chosen range of  $\lambda$  values, the effect of Gated CRF loss does not diminish significantly, possibly showing that it is less prone to loss balancing issues.

### 4.3 Comparison with the state-of-the-art

Table 5 compares our method against state-of-the-art (SOTA) weakly-supervised approaches on the Pascal VOC validation set. For all methods we report performance under weak supervision (indicated by ‘Weak’), under full supervision (indicated by ‘Full’), and we also give the ratio of the former to the latter (indicated by ‘W/F’). It is evident that for both click and scribble supervision, our method outperforms all competing approaches significantly. For instance, when clicks are used our method improves mIoU (%) over SOTA from 57.00 to 67.39, whereas for scribbles the improvement is from 72.90 to 75.50. For reference we provide the bounding-box supervised approach [29] and find that our method with only click supervision is on par, despite click being a much cheaper and weaker form of annotation. Based on the W/F ratio, which is arguably a better measure as it is independent of the selected CNN backbone in each compared approach, it can be seen that our method closes the performance gap when clicks are used, i.e. 87.88%, as well as when scribbles are used, i.e. 98.46, outperforming all SOTA approaches in this respect too. We conclude that with a proper regularization loss function, the performance gap between weak and full supervision can almost be bridged.

## 5 Conclusion

In this work, we have proposed a simple, yet effective, method for weakly supervised semantic image segmentation. The method uses the standard cross-entropy loss for labeled pixels and a novel Gated CRF loss for the unlabeled pixels. It can be trained easily with the standard Stochastic Gradient Descent method without having any pre-/post processing operations. We have presented the advantages of our loss function and what its added features bring to the problem of weakly supervised image segmentation. Finally, we have shown that our simple approach achieves state-of-the-art performance for two popular forms of weak supervision: clicks and scribbles.

**Acknowledgements:** This work is funded by Toyota Motor Europe via the research project TRACE-Zurich. We thank Fabian Mentzer and Christoph Mayer for insightful discussions.

## 6 Supplementary Materials

### 6.1 Gallery

More examples of semantic predictions with the model described in Sec. 4, trained with cross-entropy and Gated CRF losses, under different levels of supervision, are shown below.

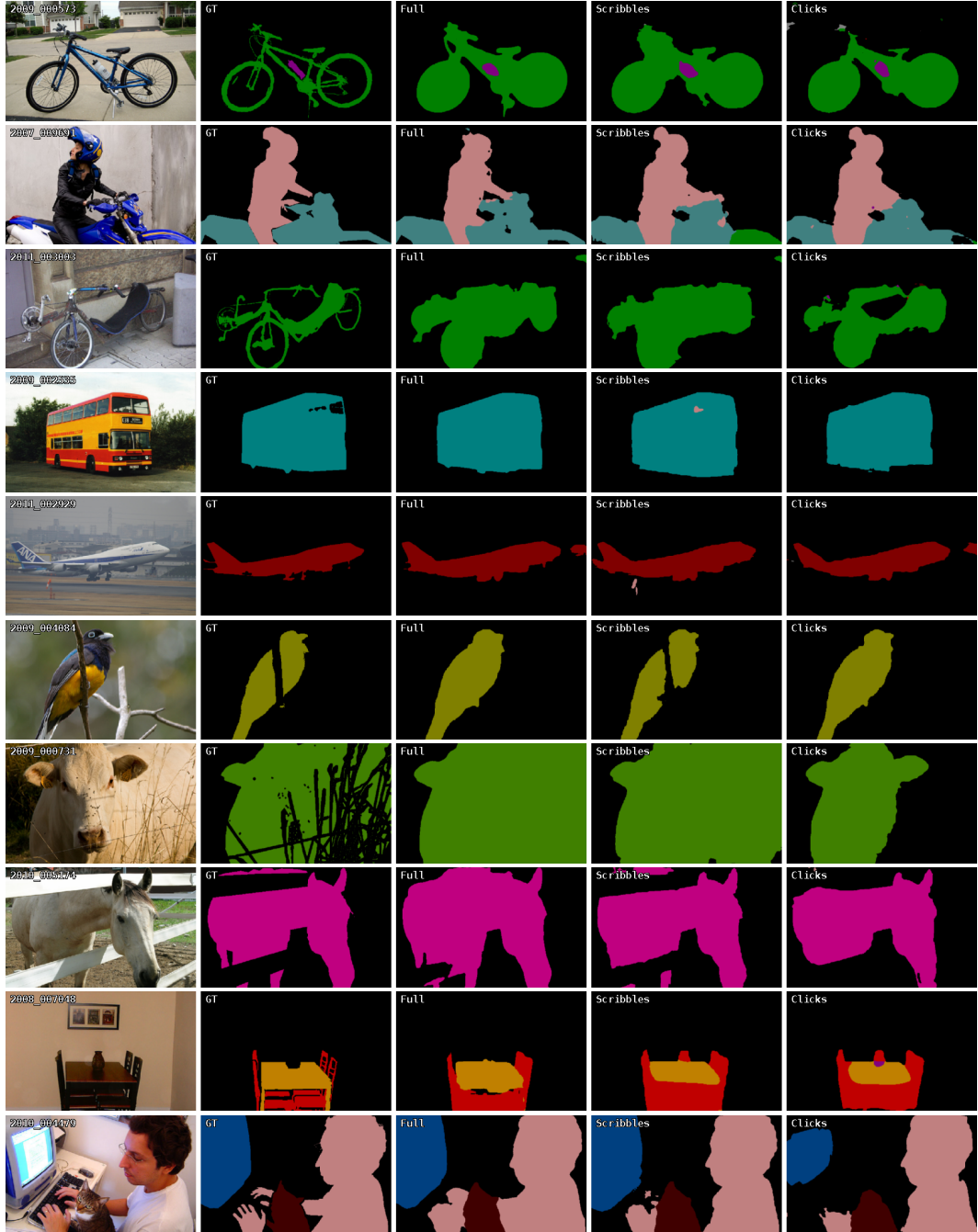


Figure 4: Left to right: Images from Pascal VOC validation set, ground truth dense annotations, predictions made by models trained with full annotations, and two models trained with weak annotations and Gated CRF loss. All models were trained on the training splits only.

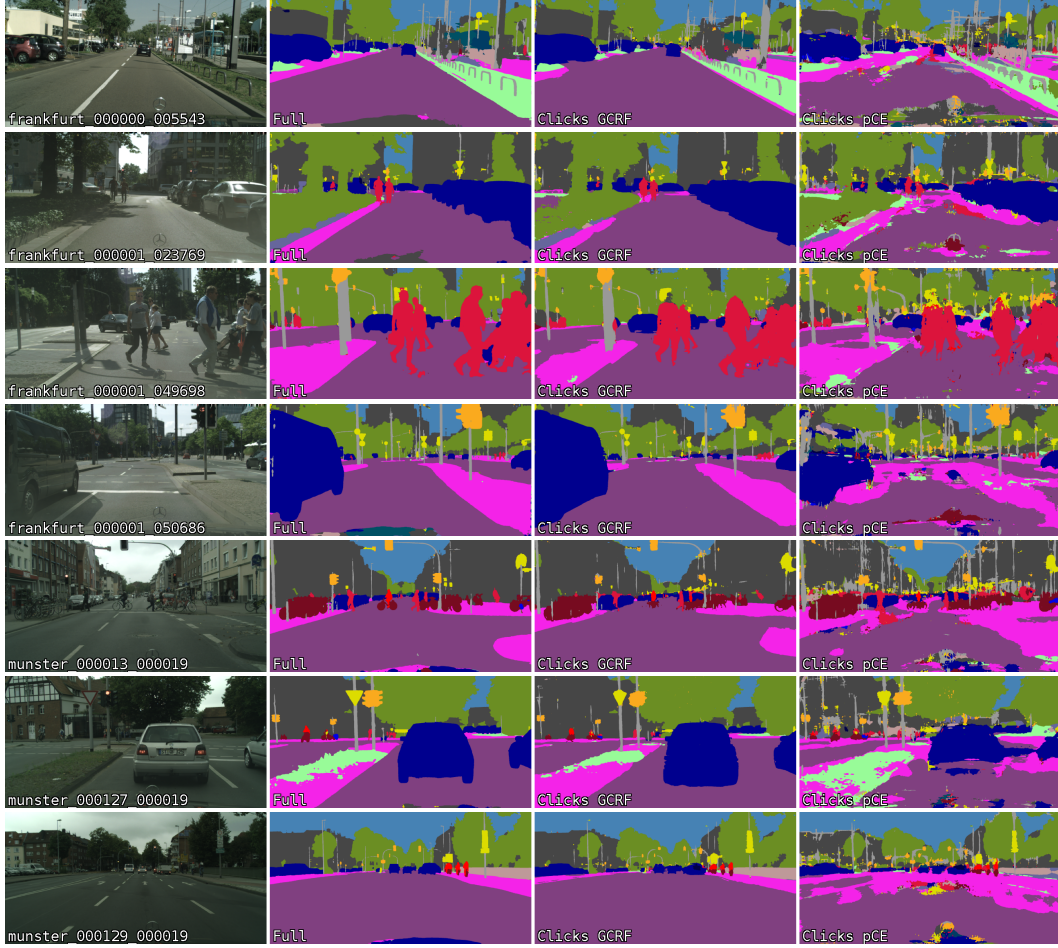


Figure 5: Left to right: Images from CityScapes validation set, predictions made by models trained with full annotations, and two models trained with clicks annotations only, with and w/o Gated CRF loss. All models were trained on the training splits only.

## 6.2 Tensor form of the Gated CRF loss

The Eq. (5) of section Method can be computed efficiently using standard tensor operations, similarly to [57]. Additionally, many packages [46] provide automatic differentiation functionality to obtain gradients of the loss function. Let  $\hat{\mathbf{Y}} \in \mathbb{R}^{H \times W \times C}$  be model prediction with probability distributions over  $C$  classes at each of  $N = HW$  pixel positions. Let  $\mathbf{M} \in \mathbb{R}^{C \times C}$  denote class compatibility matrix. Let  $\mathbf{K} \in \mathbb{R}^{R_H \times R_W \times H \times W}$  ( $R_H = R_W = 2r + 1$ ) be the aggregation of kernels  $K$ , gate function  $G$ , and  $a \neq b$  indicator:

$$\mathbf{K}_{b_y, b_x, a_y, a_x} = m_{(a_y, a_x)}^{dst} m_{(a_y - r + b_y, a_x - r + b_x)}^{src} \begin{bmatrix} b_y \neq r \\ b_x \neq r \end{bmatrix} K_{(a_y, a_x)(a_y - r + b_y, a_x - r + b_x)} \quad (6)$$

Let  $U_r : \mathbb{R}^{H \times W \times C} \rightarrow \mathbb{R}^{R_H \times R_W \times H \times W \times C}$  denote the operator, which extracts square subregions with the side  $2r + 1$  from spatial dimensions of the prediction into two new dimensions (provided as UNFOLD in [46], IM2COL elsewhere [58]):

$$U_r(\hat{\mathbf{Y}})_{b_y, b_x, a_y, a_x, c} = \hat{\mathbf{Y}}_{a_y - r + b_y, a_x - r + b_x, c} \quad (7)$$

We denote permutation, partitioning, and merging of named dimensions of a tensor  $\mathbf{X} \in \mathbb{R}^{i_1 \times i_2 \times \dots \times i_n}$  as  $\mathbf{X}_{(j_1, \dots, j_m)} \in \mathbb{R}^{j_1 \times \dots \times j_m}$  (can be composed of PERMUTE, VIEW in [46]). We denote  $\circ_b$  as Hadamard product with broadcasting along missing dimensions (C in case of tensor  $\mathbf{K}$ ). We denote  $\mathbf{J}_{s, t} \in \mathbb{R}^{s \times t}$  as a matrix of ones.

The intermediate representation of energy accumulated from source positions into valid destination positions can then be expressed as follows:

$$\Psi_D(\hat{\mathbf{Y}}) = \left[ \mathbf{K} \circ_b U_r(\hat{\mathbf{Y}}) \right]_{(HWC, R_H R_W)} \mathbf{J}_{R_H R_W, 1} \quad (8)$$

The total energy term can then be represented as follows:

$$\Psi(\hat{\mathbf{Y}}) = \mathbf{J}_{1, C} \left[ \mathbf{M} \circ \left( \hat{\mathbf{Y}}_{(C, HW)} \Psi_D(\hat{\mathbf{Y}})_{(HW, C)} \right) \right] \mathbf{J}_{C, 1} \quad (9)$$

Subsequently, the Gated CRF loss takes the following form:

$$\mathcal{L}_{GCRF}(\hat{\mathbf{Y}}) = \Psi(\hat{\mathbf{Y}}) / \sum m^{dst} \quad (10)$$

### 6.3 Simplified pairwise energy term with Potts compatibility model

The pairwise labeling energy from Eq. (3) of Method can be simplified when evaluated with Potts class compatibility model, with or without using gate function  $G$ :

$$\begin{aligned} \psi_{a,b}(\hat{y}) &= \sum_{i,j \in [1, C]} \psi_{a,b}(i, j) \hat{y}_a(i) \hat{y}_b(j) = G_{ab} K_{ab} \sum_{i=1}^C \hat{y}_a(i) \sum_{j=1}^C \mu(i, j) \hat{y}_b(j) = \\ &= G_{ab} K_{ab} \sum_{i=1}^C \hat{y}_a(i) (1 - \hat{y}_b(i)) = G_{ab} K_{ab} \left( 1 - \sum_{i=1}^C \hat{y}_a(i) \hat{y}_b(i) \right) \end{aligned} \quad (11)$$

This formulation is similar to the one used in [56, 55, 41], and may have the capacity to be implemented using the same or similar high-dimensional filtering, provided proper treatment of source and destination position maps. This study is left out of the scope of this work.

### 6.4 Detailed experimental setup

**Weak annotations for Pascal VOC.** ScribbleSup [37] presents extra annotation for all images from Pascal VOC in the form of crayon scribbles, covering all relevant classes in images. Each scribble is stored as a polyline with a class label. Following the convention by [37, 56], we rasterize this polyline with stroke width 3px. What's the point [4] authors provide another layer of annotations in the form of point coordinates, one per object instance. The only non-instance class (background) is missing from all provided point annotations, so in our experiments we simulate it from the corresponding scribble annotations of same images. We shorten polylines by 50% and consider their ends as background clicks.

**Weak annotations for CityScapes.** To mimic point annotations with CityScapes, we take instance segments annotations and apply 8-connectivity component analysis. We immediately reject components, which correspond to 'stuff' classes of size less than 256 pixels. For the left ones, if the component centroid belongs to the instance, we then take it as a click. Otherwise, we sort all pixels belonging to the component by their distance to the centroid, and take the first one that is 2.5% away from the minimum distance to the maximum. This special case handles semantic regions with holes, by placing a click point close to region center, but away from the semantic boundary. We will provide these simulated clicks as an extra layer of weak annotation to the original dataset.

**Training click annotations in CityScapes.** In case of weak supervision with point clicks, the chosen batch configurations contain more than 100 annotated points per batch on average. We have found out empirically, that such amount of supervision from pCE gives adequate results for joint training with both losses from the very beginning. However, we have observed rare cases of unstable behavior on early stages of training with CityScapes in the form of class 'road', represented by the small number of point clicks, consistently being mislabelled as 'car', of which there are multiple instances, and hence clicks, in most samples. To alleviate potential instabilities arising from early stages of training with clicks, only for this specific case we propose to: (1) weight classes when computing cross entropy, using the frequency of clicks in the batch  $w_{class} = \frac{1}{\log(1.1 + p_{class})}$  [45], and (2) perform CNN warm-up with just partial cross entropy for around 100 steps. None of these are required once cross-entropy receives supervision stronger than clicks.

## 6.5 Deliverables

**Source code.** The Gated CRF loss code will be released as a python module, implementing TORCH.NN MODULE interface.

**Datasets.** Baseline click annotations for Pascal VOC are available from the authors of [4]. Following the explanation in Sec.6.4, we will provide the complementary background clicks for Pascal VOC as WHATS\\_THE\\_POINT\\_CLICKS\\_BG.JSON, and all simulated clicks for CityScapes as CITYSCAPES\\_CLICKS.JSON along with the source code release.

## References

- [1] Andrew Adams, Jongmin Baek, and Myers Abraham Davis. Fast high-dimensional filtering using the permutohedral lattice. In *Computer Graphics Forum*, volume 29, pages 753–762, 2010.
- [2] Jiwoon Ahn and Suha Kwak. Learning pixel-level semantic affinity with image-level supervision for weakly supervised semantic segmentation. In *CVPR*, pages 4981–4990, 2018.
- [3] Vijay Badrinarayanan, Alex Kendall, and Roberto Cipolla. Segnet: A deep convolutional encoder-decoder architecture for image segmentation. *arXiv preprint arXiv:1511.00561*, 2015.
- [4] Amy Bearman, Olga Russakovsky, Vittorio Ferrari, and Li Fei-Fei. What’s the point: Semantic segmentation with point supervision. In *ECCV*, pages 549–565, 2016.
- [5] Andrew Blake and Andrew Zisserman. *Visual reconstruction*. MIT press, 1987.
- [6] Yuri Boykov and Vladimir Kolmogorov. Computing geodesics and minimal surfaces via graph cuts. In *ICCV*, page 26, 2003.
- [7] Yuri Y Boykov and M-P Jolly. Interactive graph cuts for optimal boundary & region segmentation of objects in nd images. In *ICCV*, volume 1, pages 105–112, 2001.
- [8] Vicent Caselles, Ron Kimmel, and Guillermo Sapiro. Geodesic active contours. *IJCV*, 22:61–79, 1997.
- [9] Liang-Chieh Chen, George Papandreou, Iasonas Kokkinos, Kevin Murphy, and Alan L Yuille. Deeplab: Semantic image segmentation with deep convolutional nets, atrous convolution, and fully connected crfs. *TPAMI*, 40:834–848, 2018.
- [10] Liang-Chieh Chen, George Papandreou, Florian Schroff, and Hartwig Adam. Rethinking atrous convolution for semantic image segmentation. *arXiv preprint arXiv:1706.05587*, 2017.
- [11] Liang-Chieh Chen, Yi Yang, Jiang Wang, Wei Xu, and Alan L Yuille. Attention to scale: Scale-aware semantic image segmentation. In *CVPR*, pages 3640–3649, 2016.
- [12] Liang-Chieh Chen, Yukun Zhu, George Papandreou, Florian Schroff, and Hartwig Adam. Encoder-decoder with atrous separable convolution for semantic image segmentation. *arXiv preprint arXiv:1802.02611*, 2018.
- [13] Marius Cordts, Mohamed Omran, Sebastian Ramos, Timo Rehfeld, Markus Enzweiler, Rodrigo Benenson, Uwe Franke, Stefan Roth, and Bernt Schiele. The cityscapes dataset for semantic urban scene understanding. In *CVPR*, pages 3213–3223, 2016.
- [14] Jifeng Dai, Kaiming He, and Jian Sun. Boxsup: Exploiting bounding boxes to supervise convolutional networks for semantic segmentation. In *ICCV*, pages 1635–1643, 2015.
- [15] David Eigen and Rob Fergus. Predicting depth, surface normals and semantic labels with a common multi-scale convolutional architecture. In *ICCV*, pages 2650–2658, 2015.
- [16] M. Everingham, L. Van Gool, C. K. I. Williams, J. Winn, and A. Zisserman. The PASCAL Visual Object Classes Challenge 2012 (VOC2012) Results. <http://www.pascal-network.org/challenges/VOC/voc2012/workshop/index.html>, 2012.
- [17] Stuart Geman and Donald Geman. Readings in computer vision: Issues, problems, principles, and paradigms, 1987.
- [18] Ross Girshick, Jeff Donahue, Trevor Darrell, and Jitendra Malik. Rich feature hierarchies for accurate object detection and semantic segmentation. In *CVPR*, pages 580–587, 2014.

[19] Xavier Glorot and Yoshua Bengio. Understanding the difficulty of training deep feedforward neural networks. In *Proceedings of the Thirteenth International Conference on Artificial Intelligence and Statistics*, volume 9, pages 249–256, 2010.

[20] L. Grady. Random walks for image segmentation. *TPAMI*, 28:1768–1783, 2006.

[21] Bharath Hariharan, Pablo Arbelaez, Lubomir Bourdev, Subhransu Maji, and Jitendra Malik. Semantic contours from inverse detectors. In *ICCV*, 2011.

[22] Kaiming He, Ross B. Girshick, and Piotr Dollár. Rethinking imagenet pre-training. *CoRR*, abs/1811.08883, 2018.

[23] Kaiming He, Xiangyu Zhang, Shaoqing Ren, and Jian Sun. Deep residual learning for image recognition. In *CVPR*, pages 770–778, 2016.

[24] Jie Hu, Li Shen, and Gang Sun. Squeeze-and-excitation networks. *arXiv preprint arXiv:1709.01507*, 7, 2017.

[25] Sergey Ioffe and Christian Szegedy. Batch normalization: Accelerating deep network training by reducing internal covariate shift. *CoRR*, abs/1502.03167, 2015.

[26] Thomas Joy, Alban Desmaison, Thalaiyasingam Ajanthan, Rudy Bunel, Mathieu Salzmann, Pushmeet Kohli, Philip H. S. Torr, and M. Pawan Kumar. Efficient relaxations for dense crfs with sparse higher order potentials. *CoRR*, abs/1805.09028, 2018.

[27] Michael Kass, Andrew Witkin, and Demetri Terzopoulos. Snakes: Active contour models. *IJCV*, 1:321–331, 1988.

[28] Tsung-Wei Ke, Jyh-Jing Hwang, Ziwei Liu, and Stella X Yu. Adaptive affinity fields for semantic segmentation. In *ECCV*, pages 587–602, 2018.

[29] Anna Khoreva, Rodrigo Benenson, Jan Hendrik Hosang, Matthias Hein, and Bernt Schiele. Simple does it: Weakly supervised instance and semantic segmentation. In *CVPR*, volume 1, page 3, 2017.

[30] Pushmeet Kohli, Philip HS Torr, et al. Robust higher order potentials for enforcing label consistency. *IJCV*, 82:302–324, 2009.

[31] Alexander Kolesnikov and Christoph H Lampert. Seed, expand and constrain: Three principles for weakly-supervised image segmentation. In *ECCV*, pages 695–711, 2016.

[32] Philipp Krähenbühl and Vladlen Koltun. Efficient inference in fully connected crfs with gaussian edge potentials. In *NIPS*, pages 109–117, 2011.

[33] Alex Krizhevsky, Ilya Sutskever, and Geoffrey E Hinton. Imagenet classification with deep convolutional neural networks. In *NIPS*, pages 1097–1105, 2012.

[34] John Lafferty, Andrew McCallum, and Fernando CN Pereira. Conditional random fields: Probabilistic models for segmenting and labeling sequence data, 2001.

[35] Anat Levin, Dani Lischinski, and Yair Weiss. A closed-form solution to natural image matting. *TPAMI*, 30:228–242, 2008.

[36] Yin Li, Jian Sun, Chi-Keung Tang, and Heung-Yeung Shum. Lazy snapping. In *Transactions on Graphics*, volume 23, pages 303–308, 2004.

[37] Di Lin, Jifeng Dai, Jiaya Jia, Kaiming He, and Jian Sun. Scribblesup: Scribble-supervised convolutional networks for semantic segmentation. In *CVPR*, pages 3159–3167, 2016.

[38] Tsung-Yi Lin, Michael Maire, Serge Belongie, James Hays, Pietro Perona, Deva Ramanan, Piotr Dollár, and C Lawrence Zitnick. Microsoft coco: Common objects in context. In *ECCV*, pages 740–755, 2014.

[39] Wei Liu, Andrew Rabinovich, and Alexander C Berg. Parsenet: Looking wider to see better. *arXiv preprint arXiv:1506.04579*, 2015.

[40] Jonathan Long, Evan Shelhamer, and Trevor Darrell. Fully convolutional networks for semantic segmentation. In *CVPR*, pages 3431–3440, 2015.

[41] Dmitrii Marin, Meng Tang, Ismail Ben Ayed, and Yuri Boykov. Beyond gradient descent for regularized segmentation losses. In *CVPR*, 2019.

